

1 **Long-term trends of surface ozone and its influencing factors at the**
2 **Mt. Waliguan GAW station, China, Part 1: Overall trends and**
3 **characteristics.**

4 **W. Y. Xu¹, W. L. Lin², X. B. Xu^{1,*}, J. Tang², J.Q. Huang³, H. Wu³, X.C.Zhang²**

5

6 [1] Key Laboratory for Atmospheric Chemistry, Institute of Atmospheric Composition,
7 Chinese Academy of Meteorological Sciences, Beijing, China

8 [2] Meteorological Observation Center, China Meteorological Administration, Beijing, China

9 [3] Waliguan Observatory, Qinghai Meteorological Bureau, Xining, China

10 * Correspondence to: X. B. Xu (xuxb@cams.cma.gov.cn)

11

12 **Abstract**

13 Tropospheric ozone is an important atmospheric oxidant, greenhouse gas and atmospheric
14 pollutant at the same time. The level of tropospheric ozone, particularly in the surface layer, is
15 impacted by emissions of precursors and is subjected to meteorological conditions. Due its
16 importance, the long-term variation trend of baseline ozone is highly needed for environmental
17 and climate change assessment. So far, studies about the long-term trends of ozone at
18 representative sites are mainly available for European and North American sites. Similar studies
19 are lacking for China, a country with rapid economic growth for recent decades, and many other
20 developing countries. To uncover the long-term characteristics and trends of baseline surface
21 ozone mixing ratio in western China, measurements at a global baseline Global Atmospheric
22 Watch (GAW) station in the north-eastern Tibetan Plateau region (Mt. Waliguan, 36°17' N,
23 100°54' E, 3816m a.s.l.) for the period of 1994 to 2013 were analysed in this study. Results
24 reveal higher surface ozone during the night and lower during the day at Waliguan caused by
25 mountain-valley breezes and a seasonal maximum in summer. Significant positive trends in
26 surface ozone were detected for both daytime (2.4 ± 1.6 ppbv $10a^{-1}$) and nighttime
27 (2.8 ± 1.7 ppbv $10a^{-1}$). Nighttime ozone mixing ratios are more representative of the free
28 tropospheric condition, with autumn (2.9 ± 1.1 ppbv $10a^{-1}$) and spring (2.4 ± 1.2 ppbv $10a^{-1}$)
29 revealing the largest increase rates, while summer (2.2 ± 2.0 ppbv $10a^{-1}$) and winter

1 (1.3±1.0 ppbv 10a⁻¹) show weaker increases. Spectral analysis identified four different episodes
2 with different positive trends, with the largest increase occurring around May 2000 and Oct.
3 2010. A 2-4 year, 7 year and 11 year periodicity was found in the surface ozone mixing ratio.
4 The results are highly valuable for related climate and environment change assessments of
5 western China and surrounding areas, and for the validation of chemical-climate models.

6

7 **1 Introduction**

8 Ozone (O₃) is one of the key atmospheric species and is closely related to climate change and
9 environmental issues (IPCC, 2013). The stratospheric ozone layer protects living organisms at
10 the Earth's surface against the harmful solar UV radiation, while tropospheric ozone is an
11 important greenhouse gas and governs oxidation processes in the Earth's atmosphere through
12 formation of OH radical (Stahelin et al., 2001;Lelieveld and Dentener, 2000). In the surface
13 layer, ozone is also one of the toxic gases for human beings and vegetation.

14 Since stratospheric ozone is much higher in mixing ratio than tropospheric ozone, it can be well
15 monitored by satellites with retrieved column density. However, ozone in the troposphere,
16 particularly surface ozone is highly variable in space and time. Since ozone is a secondary gas
17 pollutant, observed surface concentrations are influenced both by local photochemistry and by
18 transport processes of ozone or its precursors from nearby locations (Wang et al., 2006a;Lal et
19 al., 2014). Deep convection and stratosphere-to-troposphere exchange (STE) events can also
20 bring down ozone-rich air from above and influence surface ozone mixing ratios at high-
21 elevation sites (Bonasoni et al., 2000;Ding and Wang, 2006;Stohl et al., 2000;Tang et al.,
22 2011;Lefohn et al., 2012;Jia et al., 2015;Ma et al., 2014;Langford et al., 2009;Langford et al.,
23 2015;Lin et al., 2012a;Lin et al., 2015a). All these influencing factors make it very hard to
24 obtain the background ozone mixing ratio and to understand the causes of observed ozone
25 trends.

26 Many Global Atmosphere Watch (GAW) stations of the World Meteorological Organization
27 (WMO) and environmental monitoring sites have been setup to monitor surface ozone due to
28 its importance and due to the urgent need to evaluate the trends of background ozone. Past
29 trends in surface background ozone have been reported for Europe and North America (Cooper
30 et al., 2010;Cui et al., 2011;Gilge et al., 2010;Oltmans et al., 2013;Vingarzan, 2004;Parrish et
31 al., 2012;Logan et al., 2012), which mostly revealed strong increases in ozone before 2000 and
32 slow or even no growth afterwards. Data from some important regions, e.g., East Asia and

1 South America, are very scarce. China, as one of the rapidly developing countries, is
2 contributing increasing ozone precursor mixing ratios to the atmosphere and was thought to be
3 most responsible for the increase in ozone in the western United States (Cooper et al., 2010),
4 though other studies would suggest that STE events had an equivalent important role in causing
5 high-ozone events at western U.S. alpine sites during spring (e.g. Langford et al., 2009;
6 Ambrose et al., 2011; Lin et al., 2012a; Lin et al., 2015a). A recent study by Lin et al. (2015b)
7 found that although rising Asian emissions contribute to increasing springtime baseline ozone
8 over the western U.S. from the 1980s to the 2000s, the observed western US ozone trend over
9 the short period of 1995-2008 previously reported by Cooper et al. (2010) has been strongly
10 biased by meteorological variability and measurement sampling artefacts. Nevertheless, the
11 impact of Asian pollution outflow events on western US surface ozone is evident (Lin et al.,
12 2012b; Lin et al., 2015a).

13 Long-term trends in ozone in China, however, were seldom reported. Ding et al. (2008) studied
14 the tropospheric ozone climatology over Beijing based on aircraft data and found a 2% increase
15 of boundary layer ozone from the period of 1995-1999 to 2000-2005 in Beijing in the North
16 China Plain (NCP) region, which was mostly driven by the increasing anthropogenic emissions
17 in the surrounding regions. Upper tropospheric ozone displayed weaker increasing trends.
18 Wang et al. (2012) reported a similar increasing trend of lower tropospheric ozone and a larger
19 upper tropospheric ozone increase for the period of 2002 to 2010 based on ozonesonde
20 measurements in Beijing. Xu et al. (2008) observed positive trends and increased variability in
21 ozone at Lin'an, a background site in the Yangtze River Delta (YRD) region. Wang et al. (2009)
22 found a significant increasing trend of 0.58 ppbv yr⁻¹ during 1994 to 2007 at a coastal site of
23 Hong Kong in the Pearl River Delta (PRD) region, which were caused by rapid increases in
24 ozone precursor emissions in the upwind source regions. The above studies were all carried out
25 in the eastern part of China, in the three most polluted regions NCP, YRD and PRD, where
26 observed ozone mixing ratios were mainly under the influence of regional air pollution and are
27 not representative of the background ozone level on a larger scale. The trends of ozone over
28 other parts of China remain to be studied based on long-term observations.

29 Continuous long-term observations of surface ozone are made only at a few representative sites,
30 among which is the Mt. Waliguan (WLG) GAW station. The WLG station, established in 1994,
31 is situated in the northeastern edge of the Tibetan Plateau, where population is scarce and
32 industries hardly exist. A few studies have already been performed on short-term measurements

1 of ozone at WLG. Past research already revealed that surface ozone at the site is highly
2 representative of free-tropospheric ozone (Ma et al., 2002b) and is often influenced by
3 stratosphere-to-troposphere exchange (STE) events (Ding and Wang, 2006;Zhu et al., 2004).
4 Air masses from the west are dominant at WLG and were associated with the highest ozone
5 mixing ratios (Wang et al., 2006b). Only in summer a substantial part of the airflows come from
6 the eastern sector and exposes the surface ozone mixing ratio to some regional anthropogenic
7 influences (Wang et al., 2006b;Xue et al., 2011). Other than STE, meteorological factors with
8 very short timescales such as the diurnal cycle in topographic wind or with very long timescales
9 such as the solar cycle also have significant impacts on tropospheric ozone at WLG (Huang et
10 al., 2009;Wang et al., 2006b;Zhang et al., 2009). QBO (Quasi Bi-annual Oscillation) and ENSO
11 (El Niño and Southern Oscillation) have been shown to influence total ozone burdens over the
12 Tibet (Ji et al., 2001;Zou et al., 2001). This influence could extend to the lower troposphere via
13 STE and thus affect ozone variability measured at the 3.8 km altitude of WLG. A few studies
14 suggested that the change in dynamics after El Niño events can promote the cross-tropopause
15 ozone exchange and lead to a rise in global mean tropospheric ozone concentration (e.g.
16 Voulgarakis et al., 2011). Over western U.S. high elevation regions prone to deep stratospheric
17 intrusions, however, Lin et al. (2015a) found that the increased frequency of deep tropopause
18 folds that form in upper-level frontal zones following strong La Niña winters exerts a stronger
19 influence on springtime ozone levels at the surface than the El Niño-related increase in lower
20 stratospheric ozone burden. The Tibetan Plateau has also been identified as a preferred region
21 for deep stratospheric intrusions (Škerlak et al., 2014). The extent to which ENSO events, jet
22 characteristics and STE modulate inter-annual variability of lower tropospheric ozone at WLG
23 requires further investigation.

24 Previous studies of ozone at WLG were all based on short-term measurements and were mostly
25 model-based mechanism studies on the causes of the ozone seasonal cycle, which did not lead
26 to consensus and brought upon debates (Ma et al., 2002a;Ma et al., 2005;Zhu et al., 2004), while
27 the overall variation characteristics and long-term trend of ozone at WLG remain unclear. In
28 this study, we present an analysis of 20 year surface ozone mixing ratio at WLG. Besides
29 unravelling the characteristics of ozone variations and the overall variation trend of ozone, a
30 precise and adaptive spectral analysis method will be applied to investigate the trend during
31 different periods and the underlying periodicities within the data.

32

1 **2 Data and Methodology**

2 **2.1 Site and Measurements**

3 The Mt. Waliguan site (WLG, 36°17' N, 100°54' E, 3816 m asl) is located in Qinghai Province,
4 China. It is one of the global baseline stations of the WMO/GAW network and the only one in
5 the hinterland of Eurasia continent. WLG is situated at the northeast edge of the Qinghai-
6 Tibetan Plateau and surrounded by highland steppes, tundra, deserts, salt lakes, etc (Figure 1).
7 With very few population (about 6 persons km⁻²) and nearly no industry within 30 km, the WLG
8 site is far from major anthropogenic sources. However, some impact of long-range transport of
9 anthropogenic pollutants from the NE-SE sector cannot be excluded, particularly from the
10 major cities Xining (about 90 km northeast of WLG, population ~2.13 millions) and Lanzhou
11 (about 260 km east of WLG, population ~3.1 millions). Such impact, if any, may be significant
12 only during the warmer period (May-September), as suggested by past air mass trajectory
13 studies (Zhang et al., 2011).

14 The WLG baseline station was established in 1994. Long-term monitoring program for surface
15 ozone began in August 1994. The mixing ratio of surface ozone has been measured using two
16 ozone analysers (Model 49, Thermal Environmental Instruments; one of the analyzers was
17 replaced with a Model 49i ozone analyzer in 2011) at a sampling height of 7 meters. The
18 analysers have been automatically zeroed alternatively every second day by introducing ozone-
19 free air for 45 min. Seasonal multipoint calibrations have been done using an ozone calibrator
20 (Model 49PS, Thermal Environmental Instruments). In the years 1994, 1995, 2000, 2004, and
21 2009, the ozone calibrator and analysers at WLG were compared with the transfer standard
22 from the WMO World Calibration Centre for Surface Ozone and Carbon Monoxide, EMPA
23 Dübendorf, Switzerland. Intercomparison results show excellent or good agreement between
24 the WLG instruments and the transfer standard (Zellweger et al., 2000; Zellweger et al.,
25 2004; Zellweger et al., 2009). Surface ozone data are recorded as 5-minute averages and
26 corrected annually based on the zero-checks and multipoint calibrations. If the observed ozone
27 values from the two analysers agree within 3 ppb, average values are calculated and included
28 in the final dataset. Otherwise, causes for the differences are searched by the principal
29 investigator and only data from the well-performing analyser are included in the dataset. 5 min
30 averaged ozone mixing ratios from Aug. 1994 to Dec. 2013 were then averaged into hourly data
31 and used in this study. In the trend analysis, monthly average ozone mixing ratios were acquired

1 by first calculating the daily average ozone values and then performing a monthly averaging. A
2 data completeness of 75% was required for each averaging step.

3 Meteorological observations have been made at the site using automatic weather stations (AWS)
4 installed on the ground level and on an 80 m tower at 2, 10, 20, 40 and 80 m. These observations
5 provide meteorological parameters such as temperature, pressure, precipitation, and wind
6 speed/direction in 5 min resolution. Additionally, the vertical velocity is measured at the 80 m
7 platform. The 10 m horizontal wind and 80 m vertical wind data from Aug. 1994 to Dec. 2013
8 are used in this study and have been accordingly averaged into hourly data, which meet a data
9 completeness requirement of 75%.

10

11 **2.2 Determination of daytime and nighttime**

12 Past research has already revealed that the surface ozone at WLG is governed by different air
13 masses during daytime and nighttime (Ma et al., 2002b). The WLG station experiences upslope
14 winds during the day and is controlled by boundary layer (BL) air, while during the night, winds
15 go downslope and the site is controlled by free tropospheric (FT) air. The boundary layer air is
16 largely influenced by local photochemistry and contains pollutants transported from nearby
17 areas, while the free-tropospheric air represents the background ozone and may sometimes
18 contain signals of long-range transport or STE events. Hence, it is of necessity to differentiate
19 daytime and nighttime ozone mixing ratio in order to study the trend signals brought by
20 different air masses.

21 In the previous study (Xu et al., 2011), daytime and the nighttime were defined as a fixed time
22 ranges (e.g. 11:00-16:00 LT for daytime and 23:00-4:00 LT for nighttime). However, the actual
23 well-developed day and night time range varies with season. So does the local wind. Figures
24 2a-c respectively show the season-diurnal variation characteristics of 10 m zonal (u) and
25 meridional (v) wind velocity and the 80 m vertical (w) wind velocity. Due to the local
26 topography, the WLG station is under the influence of mountain-valley breezes and all three
27 wind vectors exhibit distinct diurnal variation characteristics. The height difference to the west
28 of Mt. WLG is much larger than that to the east, hence valley breezes during daytime come
29 from the west accompanied by upward drafts, resulting in a diurnal maximum u and w vector
30 between noontime and middle afternoon depending on season. The v vector changes from
31 southern winds to northern winds around noontime. Mountain breezes during the night come

1 from the east-south sector accompanied by subsiding air flows, resulting in low u and w and
 2 high v during the night. The dominant air flow at WLG is westerly during the cold seasons,
 3 which enhances the westerly valley breeze during the day and cancels out the easterly mountain
 4 breeze during the night. During the warm seasons, easterly winds gain in frequency, which
 5 sometimes cancels out the daytime valley breeze and enhances the nighttime mountain breeze.
 6 The distinct diurnal variation of the wind can be used to define a daytime and nighttime range
 7 that varies with season. The white dots in Figure 2 represent the monthly average occurrence
 8 hour of the diurnal maximum u . In this study, a 6 hour time range that is centred around the
 9 white dots is used as the daytime range (white dashed lines in Figure 2). The nighttime window
 10 also covers 6 h and is considered to be offset by 12 h to the daytime window.

11

12 **2.3 Trend analysis**

13 The trend analysis was performed using a both spearman's linear trend analysis and the
 14 modified Mann-Kendall's trend test. The Mann-Kendall test is performed using a Fortran
 15 program developed by Helsel et al. (2006). Here, a brief description on the modified Mann-
 16 Kendall test will be given. The Mann-Kendall test is a non-parametric test commonly used to
 17 detect trends. Hamed and Ramachandra Rao (1998) modified the test, so that it can be used on
 18 data with seasonality.

19 For two sets of observations $X = x_1, x_2, \dots, x_n$ and $Y = y_1, y_2, \dots, y_n$, the rank correlation test as
 20 proposed by (Kendall, 1955) is performed as the following:

$$21 \quad S = \sum_{i < j} a_{ij} b_{ij} \quad (1)$$

$$22 \quad \text{Where } a_{ij} = \text{sign}(x_j - x_i) = \begin{cases} 1 & x_i < x_j \\ 0 & x_i = x_j \\ -1 & x_i > x_j \end{cases} \text{ and } b_{ij} \text{ is the equivalent for } Y. \quad (2)$$

23 If Y is replaced with the time order $T = 1, 2, \dots, n$, the test becomes a trend test and $S = \sum_{i < j} a_{ij}$.
 24 The significance of the trend is tested by comparing the standardized test statistic $Z =$
 25 $S / \sqrt{\text{var}(S)}$ to the standard normal variate at a given significance level (Z_α). Here, a modified
 26 $\text{var}(S)$ is given by:

$$27 \quad \text{var}(S) = \frac{n(n-1)(2n+5)}{18} \frac{n}{n_S^*}, \quad (3)$$

1 where $\frac{n}{n_s^*}$ represents a correction for the autocorrelation that exists in the data and can be
 2 obtained by an approximation to the theoretical values.

$$3 \quad \frac{n}{n_s^*} = 1 + \frac{2}{n(n-1)(n-2)} \sum_{i=1}^n (n-i)(n-i-1)(n-i-2) \rho_s(i) \quad (4)$$

4 Here $\rho_s(i)$ is the autocorrelation function of the ranks of the observations.

5 If $|Z| > Z_{1-\alpha/2}$, then the data is non-stationary, a positive Z would indicate a positive trend and a
 6 negative Z would suggest a declining trend. If $|Z| \leq Z_{1-\alpha/2}$, then the data is stationary. Here we
 7 use $\alpha=0.05$, hence the corresponding critical $Z_{1-\alpha/2}=1.96$. A non-parametric method is then used
 8 to estimate the slope of the trend, details can be found in Sen (1968).

9

10 **2.4 The Hilbert-Huang Transform analysis**

11 The Hilbert-Huang Transform (HHT) analysis is a combination of the Empirical Mode
 12 Decomposition (EMD) and the Hilbert Spectral analysis proposed by (Huang et al., 1998). It is
 13 often used to analyse the time-frequency variation of non-linear and non-stationary processes.
 14 The EMD acts as a time-frequency filter, it decomposes the data into several oscillation modes
 15 with different characteristic time scales. The HHT method has proved to be an efficient and
 16 precise method in investigating the periodicity, long-term oscillations and trends that are
 17 embedded within the data (Huang and Wu, 2008). So far, it has been widely applied in
 18 atmospheric and climatic studies including wind field, temperature and rainfall analysis (Rao
 19 and Hsu, 2008;Lundquist, 2003;El-Askary et al., 2004), but it has not been used on atmospheric
 20 composition data yet. Here we give a brief description of the HHT method.

21 First, the EMD is performed on the data, to decompose the data into n intrinsic mode functions
 22 (IMF), c_1, c_2, \dots, c_n , and one residual r_n , which are ordered from the smallest to the largest
 23 variational time scale (Huang et al., 2003).

$$24 \quad x(t) = \sum_{j=1}^n c_j + r_n \quad (5)$$

25 Then the Hilbert transform is applied to each IMF using Eq. 6,

$$26 \quad y(t) = \frac{1}{\pi} P \int_{-\infty}^{\infty} \frac{x(t')}{t-t'} dt' \quad (6)$$

27 Where P is the Cauchy principal value. An analytical signal is then obtained with Eq.7,

$$28 \quad z(t) = x(t) + iy(t) = a(t)e^{i\theta(t)}, \quad (7)$$

1 where, $a(t) = [x^2(t) + y^2(t)]^{1/2}$ and $\theta(t) = \arctan\left(\frac{y(t)}{x(t)}\right)$. (8)

2 The instantaneous frequency ω can be calculated as the following:

3
$$\omega(t) = \frac{d\theta(t)}{dt}. \quad (9)$$

4 Thus, Eq.5 can be transformed into the following expression:

5
$$x(t) = \Re \sum_{j=1}^n a_j(t) \exp(i \int \omega_j(\tau) d\tau), \quad (10)$$

6 where \Re is the real part of the complex number.

7 To obtain the Hilbert amplitude spectrum $H(\omega, t)$, we assign for each time t , the calculated
8 amplitude $a_j(t)$ to the according $\omega_j(t)$. An integration of $H(\omega, t)$ over the frequency span would
9 yield the instantaneous energy (IE), which represents the time variation of the energy. An
10 integration along the time span would yield the marginal Hilbert spectrum $h(\omega)$, which provides
11 information on how the frequency is distributed over the entire span.

12 The degree of stationarity $DS(\omega)$ is often used to investigate the stationarity and periodicity of
13 the data, it is defined as:

14
$$DS(\omega) = \frac{1}{T} \int_0^T \left(1 - \frac{H(\omega, t)}{h(\omega)/T}\right)^2 dt, \quad (11)$$

15 where T is the entire time span.

16 The volatility which is defined as the ratio of the sum of certain IMF components $S_h(t)$ to the
17 original signal $S(t)$, here we use the summation of residual and all the IMFs but the first one as
18 $S_h(t)$:

19
$$V(t, T) = \frac{S_h(t)}{S(t)} = \frac{\sum_{j=2}^n c_j(t) + r(t)}{S(t)}, \quad (12)$$

20 where n is the number of IMFs.

21 **2.5 The gap-filling of the monthly average ozone data**

22 To perform the HHT analysis, a complete, even-spaced dataset is required. Hence we need to
23 fill the gaps in the monthly average surface ozone mixing ratio data. The location of the gaps
24 can be seen in Figure 4b. It can be noted that gaps could be found in 1997, 1998, 1999 and 2002.
25 If the gap is small and occurs in between the ozone seasonal low and peak value, then a spline
26 interpolation would suffice. However, this is not the case for some gaps. In 1997 and 1998, the

1 gaps occur during summertime, when ozone mixing ratio should be highest. In 2002, the gap
2 continues on to winter, when ozone mixing ratio should be lowest. A simple spline interpolation
3 would underestimate the seasonal peak value and overestimate the seasonal low. Hence, we
4 applied the following method to fill the gaps.

5 First, the monthly mean ozone timeseries during 1994 to 2013, as is shown in Figure 4b, is
6 shaped into an array $O_3(i,j)$ of the size [20 years \times 12 months], where $i=1994, \dots, 2013$ and
7 $j=1, \dots, 12$.

8 The gaps in $O_3(i,j)$ are filled by applying a spline interpolation on each row of the array:

$$9 \quad O_{3,spline}(1994, \dots, 2013, j) = spline(O_3(1994, \dots, 2013, j)), j = 1, \dots, 12 \quad (13)$$

10 In this way, both the average value of ozone mixing ratio at a certain month and the overall
11 ozone variation trend will be considered. A complete dataset of average monthly ozone mixing
12 ratio can then be recreated by using interpolated data only on months of missing observation
13 data:

$$14 \quad O_{3,complete} = \begin{cases} O_{3,spline}, & \text{missing } O_3 \\ O_3, & \text{existing } O_3 \end{cases} \quad (14)$$

15 The result is displayed in Figure 7a, with the original data in solid lines and interpolated data
16 in dashed lines. Our method could yield a reasonable interpolated timeseries with both seasonal
17 low and peak values occurring at the right time of year.

18 **3 Results and Discussion**

19 **3.1 Season-diurnal variation characteristics of ozone**

20 The average season-diurnal variation of surface ozone during 1994 to 2013 is displayed in
21 Figure 3. The seasonal maximum ozone occurs during summer, with an average peak in June-
22 July, while the minimum is found in winter (Figure 3a), which will be discussed in detail in
23 Section 3.2.

24 Daily maximum ozone usually occurs during nighttime, while the daily minimum ozone is
25 found around noontime, on average at 12 am, Beijing Local Time (Figure 3c). Ma et al. (2002b)
26 suggest that the WLG station is mostly influenced by boundary layer (BL) air that is brought
27 up through an upslope flow during the day, while a downslope flow brings down free
28 tropospheric (FT) air during the night. The BL air masses are typically characterised by lower

1 ozone mixing ratios in comparison with FT air masses, hence the occurrence of the daily ozone
2 minimum value indicates the time when the BL is fully developed and the air within is well
3 mixed.

4 From Figure 3b) it can be denoted that, the occurrence time of the daily minimum ozone mixing
5 ratio (red dots) shows a significant seasonal variation similar to that of the maximum zonal
6 wind velocity (white dots), with the former occurring 1-2 hours earlier than the later. Due to
7 the seasonal variation of the development of the boundary layer, the daily minimum ozone
8 should occur earlier in the day during warm seasons and later in the day during cold seasons.
9 This phenomenon can indeed be confirmed by Figure 3b), however, the ozone minimum of
10 June-August seems to occur later than expected. This phenomenon could not been found in the
11 season-diurnal variation of horizontal or vertical wind speeds, thus it is not caused by boundary
12 layer development. A possible explanation might be that the photochemical production of ozone
13 was enhanced at early noon during summertime, leading to a delayed noontime minimum. The
14 in-situ ozone production/destruction in different seasons is not well quantified at the moment.
15 Previous studies focused on modelling the photochemical net production in spring and summer
16 and reached to controversial conclusions (Ma et al., 2002b; Wang et al., 2015). Hence there is a
17 need for more investigation into the cause for such a phenomenon.

18

19 **3.2 Season-annual variation characteristics of ozone**

20 Figure 4 displays the season-annual variation of surface ozone during 1994 to 2013. Again, the
21 ozone mixing ratio peaks in summer and is lowest during winter (Fig. 4b), with an average
22 seasonal peak occurring in June during 1994 to 2013 (Fig. 4c). Previous studies reported the
23 same seasonal ozone pattern, but attributed the summertime peak to different causes, e.g., more
24 frequent STE events (Ding and Wang, 2006; Tang et al., 2011), enhanced vertical convection
25 (Ma et al., 2005), long-range transport from eastern-central China, central-southern Asia or
26 even Europe during summer (Zhu et al., 2004) and stronger cross boundary transport and
27 vertical convection during the East Asian summer monsoon season (Yang et al., 2014). From
28 Fig. 2c it can be noted that nighttime subsiding wind is indeed strongest in summer, which
29 supports the hypothesis of downward transport of ozone. Zheng et al. (2011) argue that STE
30 reaches maximum strength in spring and shows a decline in late spring based on $^{10}\text{Be}/^7\text{Be}$
31 measurements, indicating that the continuous ozone increase in summer is caused by the
32 photochemical production.

1 The long-term variation of the annual average ozone exhibits a clear increasing trend (Fig. 4a).
2 A 2-4 year cycle seems to exist within the long-term variation of surface ozone. Previous study
3 has shown that there is a quasi-biannual oscillation (QBO) within the total ozone column
4 density over the Tibetan Plateau, which is in antiphase with the QBO of the tropical
5 stratospheric winds, exhibiting a 29 month cycle (Ji et al., 2001). The influence of the QBO
6 could extend to WLG station at the 3.8 km altitude via STE. Thus, the surface ozone at WLG
7 might also have a QBO with a similar periodicity, which is related to that of the total ozone
8 column.

9 **3.3 Long-term variation trends of ozone**

10 The trends of monthly average all-day, daytime and nighttime ozone during 1994 to 2013 are
11 displayed in Figs. 5a1-c1, respectively. Ozone data in Figs. 5b1 and 5c1 are the subsets of data
12 from the daytime and nighttime ranges determined in Section 2.2 based on zonal wind
13 information. The increase in surface ozone in the past two decades is evident in all three data
14 subsets, with a slightly stronger increase in the nighttime data. The linear trends for all-day,
15 daytime and nighttime ozone mixing ratios reached 2.5, 2.4 and 2.8 ppbv $10a^{-1}$, respectively,
16 while the Kendall slopes reached 1.8, 1.7, 1.9 ppbv $10a^{-1}$, respectively. The Kendall slope is
17 smaller than the linear regression slope, mainly because the linear regression method does not
18 consider the seasonality within the data. However, both methods yielded statistically significant
19 increasing trends.

20 To further investigate the trend in ozone in different seasons, the trend of seasonal average
21 ozone during 1994 to 2013 was calculated and are shown in Figs. 5a-c (2-5). After eliminating
22 the seasonality in the data, the linear least squares fitting slopes and Kendall's slope yielded
23 very similar results, thus we only listed the linear slopes and p-values in Table 1. The strongest
24 increase in surface ozone was found in autumn (SON), followed by spring (MAM), respectively
25 reaching 2.8 and 2.4 ppbv $10a^{-1}$ in the seasonal average of all-day ozone mixing ratios. In
26 comparison, summer (JJA) and winter (DJF) both showed much weaker increasing trends, with
27 rates of 1.5 and 1.4 ppbv $10a^{-1}$, respectively, amongst which the summertime trend could not
28 even reach a confidence level of 95%. In summer the daytime increasing rate is significantly
29 lower than the nighttime one, respectively reaching 0.7 and 2.2 ppbv $10a^{-1}$. The nighttime slope
30 reached the confidence level of 95%, while the daytime slope is statistically insignificant.

1 Past investigations on the air-mass origin of WLG have shown that WLG is mostly governed
2 by western and northwestern air-masses, air-masses coming from the eastern sector takes up
3 only 2%, 5% and 8% in winter, spring and autumn, respectively (Zhang et al., 2011). However,
4 in summer there is a significant percentage (30%) of air-masses coming from the eastern
5 direction. Since the two major cities in the vicinity of WLG are both in the east, summertime is
6 believed to be the season in which WLG is most influenced by nearby anthropogenic activities.
7 From the diurnal variation of the horizontal wind speeds (Figs. 2a-b) it can be discerned that
8 daytime winds are weak northern winds, while nighttime winds are rather strong north-easterly
9 winds, which are more in favour of transporting anthropogenic pollution to WLG.

10 As already mentioned before in Section 3.2, some research believe that STE is also most
11 frequent in summer at WLG (Ding and Wang, 2006). During the night the WLG site is governed
12 by downwards winds, which may bring down air with high ozone mixing ratios from above.
13 Hence, an increase in the frequency of STE events would also result in increasing nighttime
14 ozone mixing ratios in summer. Whether it is anthropogenic activities or rather meteorological
15 factors, that has led to the distinct daytime and nighttime ozone variation slopes in summer,
16 still needs further investigations and will be discussed in Part 2 of our study.

17 The seasonal peak of the Northern Hemisphere background ozone typically occurs in spring,
18 which is believed to be the result of enhanced photochemical production in spring (Monks,
19 2000;Vingarzan, 2004). Unlike other sites in the Northern Hemisphere, the seasonal ozone peak
20 at WLG occurs during summer. However, the largest increase in ozone mixing ratio was found
21 in autumn rather than in summer. Lin et al. (2014) also reported significant increasing ozone
22 trends in autumn rather than spring at the Mauna Loa Observatory in Hawaii in the past 4
23 decades and attributed this phenomenon to strengthened ozone-rich air flows from Eurasia. The
24 reason why we observed the largest increase in ozone levels during autumn also needs further
25 exploration and will be handled in Part 2.

26 Here we present a comparison between the seasonal ozone variation trends of all the high
27 altitude (>1200 m asl) sites in the northern hemisphere (Table 2). The stations have been sorted
28 by latitude. The low latitude sites, Mauna Loa and Izaña, both show increasing trends (3.1 ± 0.7
29 and 1.4 ± 0.5 ppbv $10a^{-1}$) during 1991 to 2010 (Oltmans et al., 2013). Lin et al. (2014) suggested
30 that, in the period of 1995 to 2011 in comparison with the period of 1980 to 1995, the Mauna
31 Loa site in Hawaii displays strong increasing ozone mixing ratios during summer and autumn.
32 The mid-latitude stations exhibit inconsistent trends. Significantly positive trends were detected

1 in the Rocky Mountains, USA (3.3 ± 0.5 ppbv $10a^{-1}$, Oltmans et al., 2013) and at Jungfraujoch,
2 Switzerland (3.2 ± 1.8 ppbv $10a^{-1}$, Cui et al., 2011). Tarasova et al. (2009) found evidence for
3 increased stratospheric contribution to surface ozone at Jungfraujoch. The strongest increase at
4 Jungfraujoch was detected in winter, the weakest in summer. Gilge et al. (2010) also reported
5 increased wintertime ozone at other two alpine sites in central Europe during 1995-2007. Lin
6 et al. (2015b) reported that springtime free-tropospheric ozone displays an increasing trend of
7 0.31 ± 0.21 ppbv a^{-1} over western North America during 1995-2014, however, by shutting of
8 North American emissions in the model and focusing on the subset of ozone associated with
9 Asian influence (also possibly mixed with stratospheric intrusions), the background ozone
10 revealed a more significant increasing rate of 0.55 ± 0.14 ppbv a^{-1} during 1992-2012. No
11 significant trends were found at Pinadale, USA and Zugspitze, Germany. Negative trends were
12 revealed at Kislovodsk, Russia (-3.7 ± 1.4 ppbv $10a^{-1}$, Tarasova et al., 2009) and Whiteface,
13 USA (-2.2 ± 0.6 ppbv $10a^{-1}$, Oltmans, 2013). Tarasova et al. (2009) attributed the strong decrease
14 in ozone in Kislovodsk to control measures of Europe and the breakdown of the former USSR.
15 Both the strong increasing and decreasing trends at Jungfraujoch and Kislovodsk were mostly
16 caused by the variation in ozone mixing ratios in the 1990s. The positive trend at Jungfraujoch
17 during the 1990s was strongest in spring and weakest in summer and autumn, while the
18 reduction at Kislovodsk was strongest in summer and weaker in autumn and winter (Tarasova
19 et al., 2009). After 2000, the eastern U.S. revealed significant decrease due to the
20 implementation of NO_x emission control measures, while ozone mixing ratios at the other sites
21 in the northern mid-latitudes have entered a steady stage with either slow or no growth
22 (Tarasova et al., 2009; Oltmans et al., 2013).

23 In comparison, WLG shows a continuous rise of ozone mixing ratio throughout the past 2
24 decades and the most significant positive trends appear in autumn and spring, unlike the other
25 mid-latitude stations. The cause of this phenomenon still needs further exploration.

26 **3.4 Hilbert-Huang Spectral Analysis of surface ozone at WLG**

27 The long-term variation of surface ozone may be the result from changes in emissions of ozone
28 precursors, but may also be caused by year-to-year fluctuations or multiyear oscillations of
29 climate conditions. All the related factors have different periodicities, which is why the
30 variation of ozone is highly non-linear. To unravel the potential oscillations on different time
31 scales in the ozone timeseries, we performed an HHT analysis on the ozone data from WLG
32 using the method given in Section 2.4. The result of the EMD is shown in Fig. 6. The monthly

1 average ozone signal could be decomposed into 5 IMFs with different characteristic time scales.
2 The lowest order IMF (c1) shows an oscillation with the highest frequency. The second IMF
3 (c2) shows the seasonal variation in the ozone signal. C3 reveals 3-4 year oscillations, c4 shows
4 7 year oscillations and the highest order IMF (c5 in Fig. 6f) shows the longest oscillations
5 pattern, with a quasi-10-year periodicity.

6 Segmentations is performed by finding the local extrema of c5. The total time span could be
7 separated into 4 segments, as indicated by the dotted lines in Fig. 6a. The slope of the segments
8 of c5 can indicate whether the value is increasing or declining. To determine the significance
9 of the trend, the modified Mann-Kendall trend test is performed on each segment and the results
10 are given in Table 3. The first segment lasts 3 years (from Aug. 1994 to Jun. 1997) and reveals
11 no significant trend ($z=1.42$), with an increasing slope of $2.7 \text{ ppbv } 10\text{a}^{-1}$. The second segment
12 lasts for 5 years (from Jul. 1997 to May 2002) and displays a significant upward trend ($z=3.66$).
13 The increasing slope reaches $4.2 \text{ ppbv } 10\text{a}^{-1}$. Afterwards the increasing speed of ozone mixing
14 ratios at WLG slows down in segment 3, lasting 6 years (from Jun. 2002 to Apr. 2008), with a
15 variation slope of $3.0 \text{ ppbv } 10\text{a}^{-1}$, however, the increasing trend remains significant ($z=3.57$).
16 In the last segment, which starts in May 2008 and ends in Jul. 2013, the significant upward
17 trend continues ($z=3.65$) with a larger increasing slope ($3.6 \text{ ppbv } 10\text{a}^{-1}$) than that in segment 3.

18 Overall, surface ozone mixing ratio at WLG has been rising continuously since 1997. Figure
19 7a shows the anomaly of the interpolated monthly average ozone during 1994 to 2013, its
20 overall variation trend (represented by $c5+r$ in Fig. 6) and its variation on a scale of 7-year or
21 longer (represented by $c4+c5+r$ in Fig. 6). The corresponding variation slopes of the overall
22 variation trend and the 7-year or longer variation is depicted in Fig. 7b. The overall variation
23 trend confirms the continuous increase since Jan. 1997. The two largest slopes are respectively
24 detected in May 2000 and Oct. 2010. The 7-year or longer trend line displays a rise in ozone
25 after Aug. 1996, which reaches a maximum increasing speed in Sep. 2003. Afterwards, the
26 increase slows down and turns into a decreasing trend in Sep. 2005. After Jan. 2009, ozone
27 mixing ratios went up again, reaching a maximum increasing speed in Dec. 2010.

28 The Hilbert Energy Spectrum is depicted in Fig. 8d, along with the volatility, instantaneous
29 energy (IE) and the degree of stationarity (DS) (Figs. 8b, c, e). Both the volatility and the IE
30 reflect the variation of energy with time. Compared to the mean IE, which represents the
31 temporal variation of the frequency averaged energy, volatility rather focuses on the ratio of the
32 variation of certain signals to the total signal. Peaks in the mean IE could be found in 1994-

1 1995, 2000-2001, 2003, 2008 and 2013, which corresponds to the high ozone mixing ratio
2 values in the data. High values of volatility were found around 2003, 2008 and 2012, which
3 mostly agree with those of the IE. The cause for these high anomalies still needs to be
4 investigated upon.

5 The DS corresponding to each frequency, as displayed in Fig. 8e, can provide information on
6 the underlying periodicity within the original signal. The smaller DS is, the more stationary the
7 data is at this frequency. The lower DS values are observed in the low frequency part. A dip-
8 down at the frequencies between 0.08 and 0.12 could be found, which corresponds to the annual
9 cycle of ozone. Other dip-downs are found at even lower frequencies, corresponding to 2.5a,
10 3.5a, 7a and 11a cycles. Among all the known atmospheric factors that have an impact on the
11 ozone mixing ratio at WLG, QBO has a quasi-2-year cycle, ENSO bears a 2 to 7 year cycle and
12 solar activities vary with a 11 year cycle. The combined effect of QBO and ENSO could be
13 responsible for the 2.5a or 3.5a periodicity as suggested by the DS. Further investigations of
14 these periodicities will be carried out in Part 2.

15 **4 Summary**

16 In this paper we present the characteristics, trends and periodicity of surface ozone mixing ratio
17 at a global baseline GAW station in the eastern Tibetan Plateau region (Mt. Waliguan) during
18 the past two decades. The trends and periodicity of ozone were investigated using a modified
19 Mann-Kendall test and an adaptive method (Hilbert Huang Transform) that is suited for
20 analysing non-stationary and non-linear natural processes.

21 Results reveal that surface ozone at WLG is higher during the night and lower during the day,
22 because the station is under the control of ozone-rich free-tropospheric air during the night and
23 boundary layer air during the day due to mountain-valley breeze. Ozone displays a seasonal
24 maximum in summer and minimum in winter, which is probably caused by enhanced
25 stratosphere-to-troposphere exchange events and/or by tropospheric photochemistry. Analysis
26 suggests that there is a season-diurnal cycle in the three-dimensional winds on top of Mt.
27 Waliguan. This allows for defining well-development daytime and nighttime ranges that change
28 from month to month. Trends of surface ozone were calculated for the data subsets of the
29 defined daytime and nighttime as well as for all-day in different seasons. Both daytime and
30 nighttime surface ozone has been significantly increasing at WLG. Autumn and spring revealed
31 the largest increase rates, while summer and winter showed relatively weaker increases. A
32 significant daytime and nighttime difference in trend could only be found in summer, where

1 nighttime ozone was significantly increasing and daytime ozone bears no significant trend.
2 Summer is the season during which WLG is mostly influenced by airmasses from the eastern
3 sector. Whether anthropogenic activities in the two nearest major cities in the eastern sector
4 have impacts on the trend of summertime ozone still needs further exploration.

5 Results of the HHT spectral analysis confirm the increasing trends in surface ozone mixing
6 ratio and could further identify four different stages with different increasing rates. The overall
7 trend indicates that the largest increase occurred around May 2000 and Oct. 2010. The ozone
8 signal was also decomposed into five intrinsic mode functions with different time scales. A 2-
9 4 year, 7 year and 11 year periodicity was found within the data, the cause of which still needs
10 further investigation.

11 The results obtained in this work are very valuable for related climate and environment change
12 assessments of western China and surrounding areas, and for the validation of chemical-climate
13 models. As WLG is a high altitude mountain-top site in a remote region, measurements of
14 surface ozone and other species can well represent a large scale situation. Previous t air mass
15 origin studies and modelling studies suggest that WLG is mostly under the influence of
16 transport from the north-west direction, hence the upward trend in ozone might be a reflectance
17 upon transport from Europe (Zhang et al., 2011;Li et al., 2014). Since Eastern China is in the
18 downwind direction, our results imply that under rising background ozone conditions, even
19 more effort needs to be put in reducing ozone precursors. In the second part of our study, the
20 impact of different air-mass origins and the long-term variations of their occurrence frequencies
21 on the surface ozone mixing ratio and its trend at WLG will be shown. The anthropogenic
22 impact of the nearest major population centers on the ozone trend will be discussed. The long-
23 term variation of STE and its link to surface ozone at WLG will be displayed. The possible
24 connection of changes in atmospheric circulation oscillations and solar activities with the inner-
25 annual and periodical variations of ozone at WLG will be studied.

26

27 **Acknowledgements**

28 We thank all operators of the Mt. Waliguan Baseline Station for their excellent routine work.
29 We appreciate WMO/GEF, WMO/GAW, Canada/AES, and Swiss/WCC-Empa for funding and
30 technical support. This work is supported by China Special Fund for Meteorological Research
31 in the Public Interest (No. GYHY201106023), China Special Fund for Environmental Research

1 in the Public Interest (No. 201509002), the Basic Research Fund of CAMS (No. 2013Z005)
2 and the Natural Science Foundation of China (No. 21177157).
3

1 **References**

2

- 3 Ambrose, J. L., Reidmiller, D. R., and Jaffe, D. A.: Causes of high O₃ in the lower free
4 troposphere over the Pacific Northwest as observed at the Mt. Bachelor Observatory,
5 *Atmospheric Environment*, 45, 5302-5315, <http://dx.doi.org/10.1016/j.atmosenv.2011.06.056>,
6 2011.
- 7 Bonasoni, P., Evangelisti, F., Bonafe, U., Ravegnani, F., Calzolari, F., Stohl, A., Tositti, L.,
8 Tubertini, O., and Colombo, T.: Stratospheric ozone intrusion episodes recorded at Mt. Cimone
9 during the VOTALP project: case studies, *Atmospheric Environment*, 34, 1355-1365,
10 [http://dx.doi.org/10.1016/S1352-2310\(99\)00280-0](http://dx.doi.org/10.1016/S1352-2310(99)00280-0), 2000.
- 11 Cooper, O. R., Parrish, D. D., Stohl, A., Trainer, M., Nedelec, P., Thouret, V., Cammas, J. P.,
12 Oltmans, S. J., Johnson, B. J., Tarasick, D., Leblanc, T., McDermid, I. S., Jaffe, D., Gao, R.,
13 Stith, J., Ryerson, T., Aikin, K., Campos, T., Weinheimer, A., and Avery, M. A.: Increasing
14 springtime ozone mixing ratios in the free troposphere over western North America, *Nature*,
15 463, 344-348, 10.1038/nature08708, 2010.
- 16 Cui, J., Pandey Deolal, S., Sprenger, M., Henne, S., Staehelin, J., Steinbacher, M., and Nédélec,
17 P.: Free tropospheric ozone changes over Europe as observed at Jungfraujoch (1990–2008): An
18 analysis based on backward trajectories, *Journal of Geophysical Research: Atmospheres*, 116,
19 n/a-n/a, 10.1029/2010JD015154, 2011.
- 20 Ding, A., and Wang, T.: Influence of stratosphere-to-troposphere exchange on the seasonal
21 cycle of surface ozone at Mount Waliguan in western China, *Geophysical Research Letters*, 33,
22 L03803, 10.1029/2005GL024760, 2006.
- 23 Ding, A. J., Wang, T., Thouret, V., Cammas, J. P., and Nédélec, P.: Tropospheric ozone
24 climatology over Beijing: analysis of aircraft data from the MOZAIC program, *Atmos. Chem.*
25 *Phys.*, 8, 1-13, 10.5194/acp-8-1-2008, 2008.
- 26 El-Askary, H., Sarkar, S., Chiu, L., Kafatos, M., and El-Ghazawi, T.: Rain gauge derived
27 precipitation variability over Virginia and its relation with the El Nino southern oscillation,
28 *Advances in Space Research*, 33, 338-342, [http://dx.doi.org/10.1016/S0273-1177\(03\)00478-2](http://dx.doi.org/10.1016/S0273-1177(03)00478-2),
29 2004.
- 30 Gilge, S., Plass-Duelmer, C., Fricke, W., Kaiser, A., Ries, L., Buchmann, B., and Steinbacher,
31 M.: Ozone, carbon monoxide and nitrogen oxides time series at four alpine GAW mountain
32 stations in central Europe, *Atmos. Chem. Phys.*, 10, 12295-12316, 10.5194/acp-10-12295-2010,
33 2010.
- 34 Hamed, K. H., and Ramachandra Rao, A.: A modified Mann-Kendall trend test for
35 autocorrelated data, *Journal of Hydrology*, 204, 182-196, [http://dx.doi.org/10.1016/S0022-](http://dx.doi.org/10.1016/S0022-1694(97)00125-X)
36 [1694\(97\)00125-X](http://dx.doi.org/10.1016/S0022-1694(97)00125-X), 1998.
- 37 Helsel, D. R., Mueller, D. K., and Slack, J. R.: Computer program for the Kendall family of
38 trend tests: U.S. Geological Survey Scientific Investigations Report 2005-5275, 4p.b,
39 <http://pubs.usgs.gov/sir/2005/5275/pdf/sir2005-5275.pdf>, 2006.
- 40 Huang, F.-X., Liu, N.-Q., and Zhao, M.-X.: Solar Cycle Signal of Tropospheric Ozone over the
41 Tibetan Plateau, *Chinese Journal of Geophysics*, 52, 913-921, 10.1002/cjg2.1416, 2009.

1 Huang, N. E., Shen, Z., Long, S. R., Wu, M. C., Shih, H. H., Zheng, Q., Yen, N.-C., Tung, C.
2 C., and Liu, H. H.: The empirical mode decomposition and the Hilbert spectrum for nonlinear
3 and non-stationary time series analysis, 1971, 903-995 pp., 1998.

4 Huang, N. E., Wu, M.-L. C., Long, S. R., Shen, S. S. P., Qu, W., Gloersen, P., and Fan, K. L.:
5 A confidence limit for the empirical mode decomposition and Hilbert spectral analysis, 2037,
6 2317-2345 pp., 2003.

7 Huang, N. E., and Wu, Z.: A review on Hilbert-Huang transform: Method and its applications
8 to geophysical studies, *Reviews of Geophysics*, 46, RG2006, 10.1029/2007RG000228, 2008.

9 IPCC: Climate Change 2013: The Physical Science Basis. Contribution of Working Group I to
10 the Fifth Assessment Report of the Intergovernmental Panel on Climate Change, Cambridge
11 Univ. Press, Cambridge, United Kingdom and New York, NY, USA, 1535, 2013.

12 Ji, C. P., Zou, H., and Zhou, L. B.: QBO Signal in Total Ozone Over the Tibet, *Climatic and*
13 *Environmental Research*, 6, 416-424, 2001.

14 Jia, S., Xu, X., Lin, W., Wang, Y., He, X., and Zhang, H.: Increased mixing ratio of surface
15 ozone by nighttime convection process over the North China Plain, *Journal of Applied*
16 *Meteorological Science*, 26, 280-290, 2015.

17 Kendall, M. G.: Rank Correlation Methods, Charles Griffin, London, 1955.

18 Lal, S., Venkataramani, S., Chandra, N., Cooper, O. R., Brioude, J., and Naja, M.: Transport
19 effects on the vertical distribution of tropospheric ozone over western India, *Journal of*
20 *Geophysical Research: Atmospheres*, 2014JD021854, 10.1002/2014JD021854, 2014.

21 Langford, A. O., Aikin, K. C., Eubank, C. S., and Williams, E. J.: Stratospheric contribution to
22 high surface ozone in Colorado during springtime, *Geophysical Research Letters*, 36, n/a-n/a,
23 10.1029/2009GL038367, 2009.

24 Langford, A. O., Senff, C. J., Alvarez Ii, R. J., Brioude, J., Cooper, O. R., Holloway, J. S., Lin,
25 M. Y., Marchbanks, R. D., Pierce, R. B., Sandberg, S. P., Weickmann, A. M., and Williams, E.
26 J.: An overview of the 2013 Las Vegas Ozone Study (LVOS): Impact of stratospheric intrusions
27 and long-range transport on surface air quality, *Atmospheric Environment*, 109, 305-322,
28 <http://dx.doi.org/10.1016/j.atmosenv.2014.08.040>, 2015.

29 Lefohn, A. S., Wernli, H., Shadwick, D., Oltmans, S. J., and Shapiro, M.: Quantifying the
30 importance of stratospheric-tropospheric transport on surface ozone concentrations at high- and
31 low-elevation monitoring sites in the United States, *Atmospheric Environment*, 62, 646-656,
32 <http://dx.doi.org/10.1016/j.atmosenv.2012.09.004>, 2012.

33 Lelieveld, J., and Dentener, F. J.: What controls tropospheric ozone?, *Journal of Geophysical*
34 *Research: Atmospheres*, 105, 3531-3551, 10.1029/1999JD901011, 2000.

35 Li, X., Liu, J., Mauzerall, D. L., Emmons, L. K., Walters, S., Horowitz, L. W., and Tao, S.:
36 Effects of trans-Eurasian transport of air pollutants on surface ozone concentrations over
37 Western China, *Journal of Geophysical Research: Atmospheres*, 119, 12,338-312,354,
38 10.1002/2014JD021936, 2014.

39 Lin, M., Fiore, A. M., Cooper, O. R., Horowitz, L. W., Langford, A. O., Levy, H., Johnson, B.
40 J., Naik, V., Oltmans, S. J., and Senff, C. J.: Springtime high surface ozone events over the
41 western United States: Quantifying the role of stratospheric intrusions, *Journal of Geophysical*
42 *Research: Atmospheres*, 117, n/a-n/a, 10.1029/2012JD018151, 2012a.

- 1 Lin, M., Fiore, A. M., Horowitz, L. W., Cooper, O. R., Naik, V., Holloway, J., Johnson, B. J.,
2 Middlebrook, A. M., Oltmans, S. J., Pollack, I. B., Ryerson, T. B., Warner, J. X., Wiedinmyer,
3 C., Wilson, J., and Wyman, B.: Transport of Asian ozone pollution into surface air over the
4 western United States in spring, *Journal of Geophysical Research: Atmospheres*, 117, n/a-n/a,
5 10.1029/2011JD016961, 2012b.
- 6 Lin, M., Horowitz, L. W., Oltmans, S. J., Fiore, A. M., and Fan, S.: Tropospheric ozone trends
7 at Mauna Loa Observatory tied to decadal climate variability, *Nature Geosci*, 7, 136-143,
8 10.1038/ngeo2066, 2014.
- 9 Lin, M., Fiore, A. M., Horowitz, L. W., Langford, A. O., Oltmans, S. J., Tarasick, D., and
10 Rieder, H. E.: Climate variability modulates western US ozone air quality in spring via deep
11 stratospheric intrusions, *Nat Commun*, 6, 10.1038/ncomms8105, 2015a.
- 12 Lin, M., Horowitz, L. W., Cooper, O. R., Tarasick, D., Conley, S., Iraci, L. T., Johnson, B.,
13 Leblanc, T., Petropavlovskikh, I., and Yates, E. L.: Revisiting the evidence of increasing
14 springtime ozone mixing ratios in the free troposphere over western North America,
15 *Geophysical Research Letters*, n/a-n/a, 10.1002/2015GL065311, 2015b.
- 16 Logan, J. A., Staehelin, J., Megretskaia, I. A., Cammas, J. P., Thouret, V., Claude, H., De
17 Backer, H., Steinbacher, M., Scheel, H. E., Stübi, R., Fröhlich, M., and Derwent, R.: Changes
18 in ozone over Europe: Analysis of ozone measurements from sondes, regular aircraft (MOZAIC)
19 and alpine surface sites, *Journal of Geophysical Research: Atmospheres*, 117, D09301,
20 10.1029/2011JD016952, 2012.
- 21 Lundquist, J. K.: Intermittent and Elliptical Inertial Oscillations in the Atmospheric Boundary
22 Layer, *Journal of the Atmospheric Sciences*, 60, 2661-2673, 10.1175/1520-
23 0469(2003)060<2661:IAEIOI>2.0.CO;2, 2003.
- 24 Ma, J., Liu, H., and Hauglustaine, D.: Summertime tropospheric ozone over China simulated
25 with a regional chemical transport model 1. Model description and evaluation, *Journal of*
26 *Geophysical Research: Atmospheres*, 107, ACH 27-21-ACH 27-13, 10.1029/2001JD001354,
27 2002a.
- 28 Ma, J., Tang, J., Zhou, X., and Zhang, X.: Estimates of the Chemical Budget for Ozone at
29 Waliguan Observatory, *Journal of Atmospheric Chemistry*, 41, 21-48,
30 10.1023/A:1013892308983, 2002b.
- 31 Ma, J., Zheng, X., and Xu, X.: Comment on “Why does surface ozone peak in summertime at
32 Waliguan?” by Bin Zhu et al, *Geophysical Research Letters*, 32, n/a-n/a,
33 10.1029/2004GL021683, 2005.
- 34 Ma, J., Lin, W. L., Zheng, X. D., Xu, X. B., Li, Z., and Yang, L. L.: Influence of air mass
35 downward transport on the variability of surface ozone at Xianggelila Regional Atmosphere
36 Background Station, southwest China, *Atmos. Chem. Phys.*, 14, 5311-5325, 10.5194/acp-14-
37 5311-2014, 2014.
- 38 Monks, P. S.: A review of the observations and origins of the spring ozone maximum,
39 *Atmospheric Environment*, 34, 3545-3561, [http://dx.doi.org/10.1016/S1352-2310\(00\)00129-1](http://dx.doi.org/10.1016/S1352-2310(00)00129-1),
40 2000.
- 41 Oltmans, S. J., Lefohn, A. S., Shadwick, D., Harris, J. M., Scheel, H. E., Galbally, I., Tarasick,
42 D. W., Johnson, B. J., Brunke, E. G., Claude, H., Zeng, G., Nichol, S., Schmidlin, F., Davies,
43 J., Cuevas, E., Redondas, A., Naoe, H., Nakano, T., and Kawasato, T.: Recent tropospheric

- 1 ozone changes – A pattern dominated by slow or no growth, *Atmospheric Environment*, 67,
2 331-351, <http://dx.doi.org/10.1016/j.atmosenv.2012.10.057>, 2013.
- 3 Parrish, D. D., Law, K. S., Staehelin, J., Derwent, R., Cooper, O. R., Tanimoto, H., Volz-
4 Thomas, A., Gilge, S., Scheel, H. E., Steinbacher, M., and Chan, E.: Long-term changes in
5 lower tropospheric baseline ozone concentrations at northern mid-latitudes, *Atmos. Chem.*
6 *Phys.*, 12, 11485-11504, 10.5194/acp-12-11485-2012, 2012.
- 7 Rao, A. R., and Hsu, E.-C.: *Hilbert-Huang Transform Analysis of Hydrological and*
8 *Environmental Time Series*, 1 ed., Water Science and Technology Library, 60, Springer
9 Netherlands, 2008.
- 10 Sen, P. K.: Estimates of the regression coefficient based on Kendall's tau, *Journal of the*
11 *American Statistical Association*, 63, 1379-1389, 1968.
- 12 Škerlak, B., Sprenger, M., and Wernli, H.: A global climatology of stratosphere–troposphere
13 exchange using the ERA-Interim data set from 1979 to 2011, *Atmos. Chem. Phys.*, 14, 913-
14 937, 10.5194/acp-14-913-2014, 2014.
- 15 Staehelin, J., Harris, N. R. P., Appenzeller, C., and Eberhard, J.: Ozone trends: A review,
16 *Reviews of Geophysics*, 39, 231-290, 10.1029/1999RG000059, 2001.
- 17 Stohl, A., Spichtinger-Rakowsky, N., Bonasoni, P., Feldmann, H., Memmesheimer, M., Scheel,
18 H. E., Trickl, T., Hübener, S., Ringer, W., and Mandl, M.: The influence of stratospheric
19 intrusions on alpine ozone concentrations, *Atmospheric Environment*, 34, 1323-1354,
20 [http://dx.doi.org/10.1016/S1352-2310\(99\)00320-9](http://dx.doi.org/10.1016/S1352-2310(99)00320-9), 2000.
- 21 Tang, Q., Prather, M. J., and Hsu, J.: Stratosphere-troposphere exchange ozone flux related to
22 deep convection, *Geophys. Res. Lett.*, 38, L03806, 10.1029/2010gl046039, 2011.
- 23 Tarasova, O. A., Senik, I. A., Sosonkin, M. G., Cui, J., Staehelin, J., and Prévôt, A. S. H.:
24 Surface ozone at the Caucasian site Kislovodsk High Mountain Station and the Swiss Alpine
25 site Jungfraujoch: data analysis and trends (1990–2006), *Atmos. Chem. Phys.*, 9, 4157-4175,
26 10.5194/acp-9-4157-2009, 2009.
- 27 Vingarzan, R.: A review of surface ozone background levels and trends, *Atmospheric*
28 *Environment*, 38, 3431-3442, <http://dx.doi.org/10.1016/j.atmosenv.2004.03.030>, 2004.
- 29 Voulgarakis, A., Hadjinicolaou, P., and Pyle, J. A.: Increases in global tropospheric ozone
30 following an El Niño event: examining stratospheric ozone variability as a potential driver,
31 *Atmospheric Science Letters*, 12, 228-232, 10.1002/asl.318, 2011.
- 32 Wang, Q. Y., Gao, R. S., Cao, J. J., Schwarz, J. P., Fahey, D. W., Shen, Z. X., Hu, T. F., Wang,
33 P., Xu, X. B., and Huang, R. J.: Observations of high level of ozone at Qinghai Lake basin in
34 the northeastern Qinghai-Tibetan Plateau, western China, *Journal of Atmospheric Chemistry*,
35 72, 19-26, 10.1007/s10874-015-9301-9, 2015.
- 36 Wang, T., Ding, A., Gao, J., and Wu, W. S.: Strong ozone production in urban plumes from
37 Beijing, China, *Geophys. Res. Lett.*, 33, L21806, 10.1029/2006gl027689, 2006a.
- 38 Wang, T., Wong, H. L. A., Tang, J., Ding, A., Wu, W. S., and Zhang, X. C.: On the origin of
39 surface ozone and reactive nitrogen observed at a remote mountain site in the northeastern
40 Qinghai-Tibetan Plateau, western China, *Journal of Geophysical Research: Atmospheres*, 111,
41 D08303, 10.1029/2005JD006527, 2006b.

- 1 Wang, T., Wei, X. L., Ding, A. J., Poon, C. N., Lam, K. S., Li, Y. S., Chan, L. Y., and Anson,
2 M.: Increasing surface ozone concentrations in the background atmosphere of Southern China,
3 1994–2007, *Atmos. Chem. Phys.*, 9, 6217–6227, 10.5194/acp-9-6217-2009, 2009.
- 4 Wang, Y., Konopka, P., Liu, Y., Chen, H., Müller, R., Plöger, F., Riese, M., Cai, Z., and Lü,
5 D.: Tropospheric ozone trend over Beijing from 2002–2010: ozonesonde measurements and
6 modeling analysis, *Atmos. Chem. Phys.*, 12, 8389–8399, 10.5194/acp-12-8389-2012, 2012.
- 7 Xu, X., Lin, W., Wang, T., Yan, P., Tang, J., Meng, Z., and Wang, Y.: Long-term trend of
8 surface ozone at a regional background station in eastern China 1991–2006: enhanced
9 variability, *Atmos. Chem. Phys.*, 8, 2595–2607, 10.5194/acp-8-2595-2008, 2008.
- 10 Xue, L. K., Wang, T., Zhang, J. M., Zhang, X. C., Deliger, Poon, C. N., Ding, A. J., Zhou, X.
11 H., Wu, W. S., Tang, J., Zhang, Q. Z., and Wang, W. X.: Source of surface ozone and reactive
12 nitrogen speciation at Mount Waliguan in western China: New insights from the 2006 summer
13 study, *J. Geophys. Res.*, 116, D07306, 10.1029/2010jd014735, 2011.
- 14 Yang, Y., Liao, H., and Li, J.: Impacts of the East Asian summer monsoon on interannual
15 variations of summertime surface-layer ozone concentrations over China, *Atmos. Chem. Phys.*,
16 14, 6867–6879, 10.5194/acp-14-6867-2014, 2014.
- 17 Zellweger, C., Hofer, P., and Buchmann, B.: System and Performance Audit of Surface Ozone
18 and Carbon Monoxide at the China GAW Baseline Observatory Waliguan Mountain, WCC-
19 Empa Report 00/3Rep., 46 pp, Empa, Dübendorf, Switzerland,
20 http://gaw.empa.ch/audits/WLG_2000.pdf, 2000.
- 21 Zellweger, C., Klausen, J., and Buchmann, B.: System and Performance Audit of Surface
22 Ozone Carbon Monoxide and Methane at the Global GAW Station Mt. Waliguan, China,
23 October 2004, WCC-Empa Report 04/3Rep., 52 pp, Empa, Dübendorf, Switzerland,
24 http://gaw.empa.ch/audits/WLG_2004.pdf, 2004.
- 25 Zellweger, C., Klausen, J., Buchmann, B., and Scheel, H.-E.: System and Performance Audit
26 of Surface Ozone, Carbon Monoxide, Methane and Nitrous Oxide at the GAW Global Station
27 Mt. Waliguan and the Chinese Academy of Meteorological Sciences (CAMS) China, June 2009,
28 WCC-Empa Report 09/2Rep., 61 pp, Empa, Dübendorf, Switzerland,
29 https://www.wmo.int/pages/prog/arep/gaw/documents/WLG_2009.pdf, 2009.
- 30 Zhang, F., Zhou, L. X., Novelli, P. C., Worthy, D. E. J., Zellweger, C., Klausen, J., Ernst, M.,
31 Steinbacher, M., Cai, Y. X., Xu, L., Fang, S. X., and Yao, B.: Evaluation of in situ
32 measurements of atmospheric carbon monoxide at Mount Waliguan, China, *Atmos. Chem.*
33 *Phys.*, 11, 5195–5206, 10.5194/acp-11-5195-2011, 2011.
- 34 Zhang, J. M., Wang, T., Ding, A. J., Zhou, X. H., Xue, L. K., Poon, C. N., Wu, W. S., Gao, J.,
35 Zuo, H. C., Chen, J. M., Zhang, X. C., and Fan, S. J.: Continuous measurement of peroxyacetyl
36 nitrate (PAN) in suburban and remote areas of western China, *Atmospheric Environment*, 43,
37 228–237, 10.1016/j.atmosenv.2008.09.070, 2009.
- 38 Zheng, X. D., Shen, C. D., Wan, G. J., Liu, K. X., Tang, J., and Xu, X. B.: $\sim(10)\text{Be}/\sim 7\text{Be}$
39 implies the contribution of stratosphere-troposphere transport to the winter-spring surface O_3
40 variation observed on the Tibetan Plateau, *Chin. Sci. Bull.*, 56, 84–88, 2011.
- 41 Zhu, B., Akimoto, H., Wang, Z., Sudo, K., Tang, J., and Uno, I.: Why does surface ozone peak
42 in summertime at Waliguan?, *Geophysical Research Letters*, 31, L17104,
43 10.1029/2004GL020609, 2004.

1 Zou, H., Ji, C. P., Zhou, L. B., Wang, W., and Jiang, Y. X.: ENSO Signal in Total Ozone over
2 Tibet, Climatic and Environmental Research, 6, 267-272, 2001.
3
4

1 Table 1 The linear slope, 95% confidence interval (in ppbv 10a⁻¹) and the p-values (in
 2 parenthesis) of seasonal average surface ozone mixing ratio during 1994 to 2013

Data subset	MAM	JJA	SON	DJF
All Day	2.4±1.1 (<0.01)	1.5±1.9 (0.12)	2.8±1.1 (<0.01)	1.4±0.9 (<0.01)
Day	2.4±1.1 (<0.01)	0.7±1.8 (0.41)	2.7±1.0 (<0.01)	1.5±0.9 (<0.01)
Night	2.4±1.2 (<0.01)	2.2±2.0 (0.04)	2.9±1.1 (<0.01)	1.3±1.0 (0.01)

3
4

1

2 Table 2 The linear slope (in ppbv 10a⁻¹) and the 95% confidence interval of all-year and
 3 seasonal average surface ozone mixing ratio during 1994 to 2013 at north hemispheric high
 4 altitude GAW sites.

Station (Location)	Time Span	All Year	MAM	JJA	SON	DJF	Reference
Mauna Loa, USA (19.5N, 155.6W, 3397 m asl)	1991-2010	3.1±0.7					(Oltmans et al., 2013)
Izaña, Spain (28.3N, 16.5W, 2367 m asl)	1991-2010	1.4±0.5					(Oltmans et al., 2013)
Waliguan, China (36.3N, 100.9E, 3816 m asl)	1994-2013	2.5±1.7	2.4±1.1	1.5±1.9	2.8±1.1	1.4 ±0.9	This work
Rocky, USA (40.3N, 105.6W, 2743 m asl)	1991-2010	3.3±0.5					(Oltmans et al., 2013)
Pinadale, USA (42.9N, 109.8W, 2743 m asl)	1991-2010	-0.5±0.4					(Oltmans et al., 2013)
Kislovodsk, Russia (43.70N, 42.70E, 2070 m asl)	1991-2006	-3.7±1.4	-2.0±2.0	-1.4±2.4	-6.0±2.1	-3.0±2.5	(Tarasova et al., 2009)
Whiteface, USA (44.4N, 73.9W, 1484 m asl)	1991-2010	-2.2±0.6					(Oltmans et al., 2013)
Jungfrauoch, Switzerland (46.5N, 8.0E, 3580 m asl)	1990-2008	3.2±1.8	3.3±2.2	2.2±2.8	3.3±1.6	4.9±1.7	(Cui et al., 2011)
Zugspitze, Germany (47.4N, 11.0E, 2960 m asl)	1991-2010	0.5±0.4					(Oltmans et al., 2013)

5

6

1

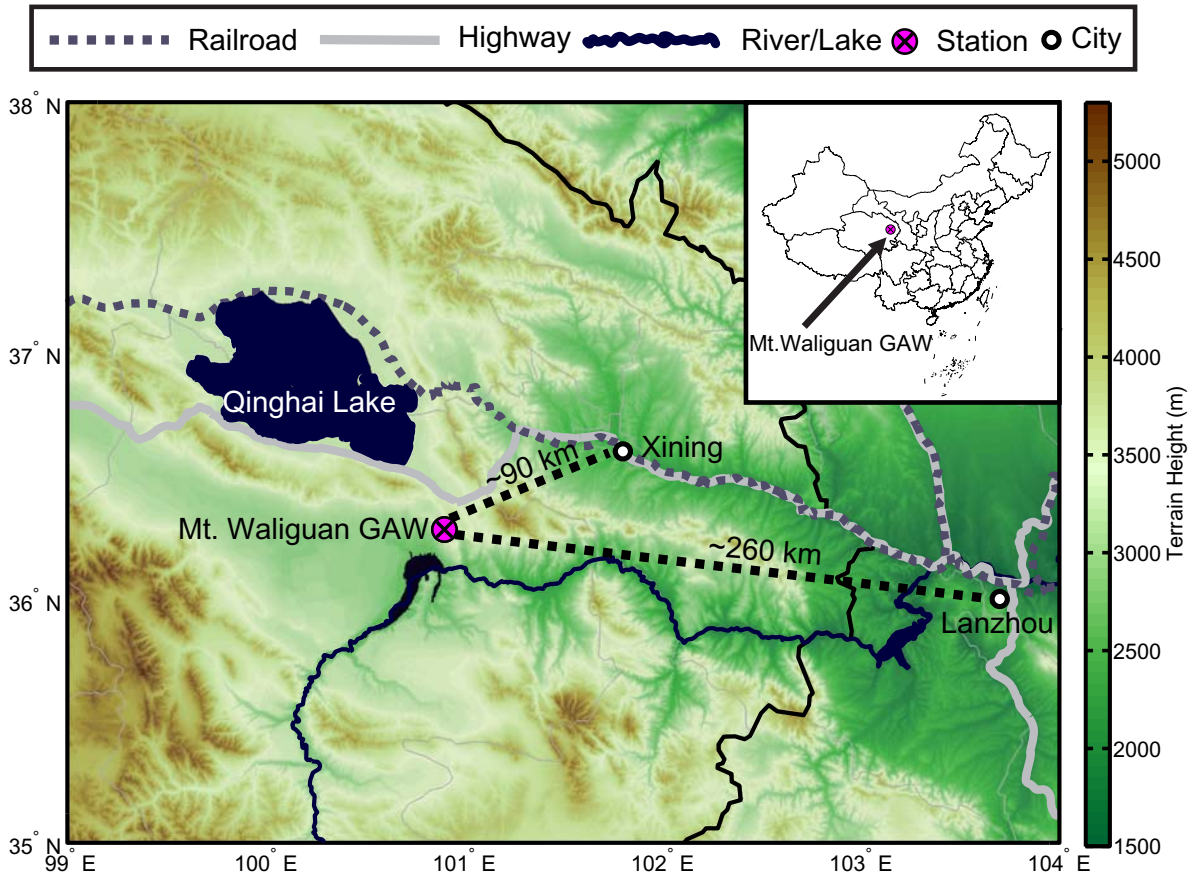
2 Table 3 Modified Mann-Kendall trend test on segments based on the last IMF.

Segment	Time Range	Slope of c5	Modified Mann-Kendall test (z)	Slope of O ₃ (ppbv 10a ⁻¹)
1	Aug1994- Jun1997	-	No significant trend (z =1.42)	2.7
2	Jul1997-May2002	+	Significant upward trend (z =3.66)	4.2
3	Jun2002-Apr2008	-	Significant upward trend (z =3.57)	3.0
4	May2008-Jul2013	+	Significant upward trend (z = 3.42)	3.6

3

4

1

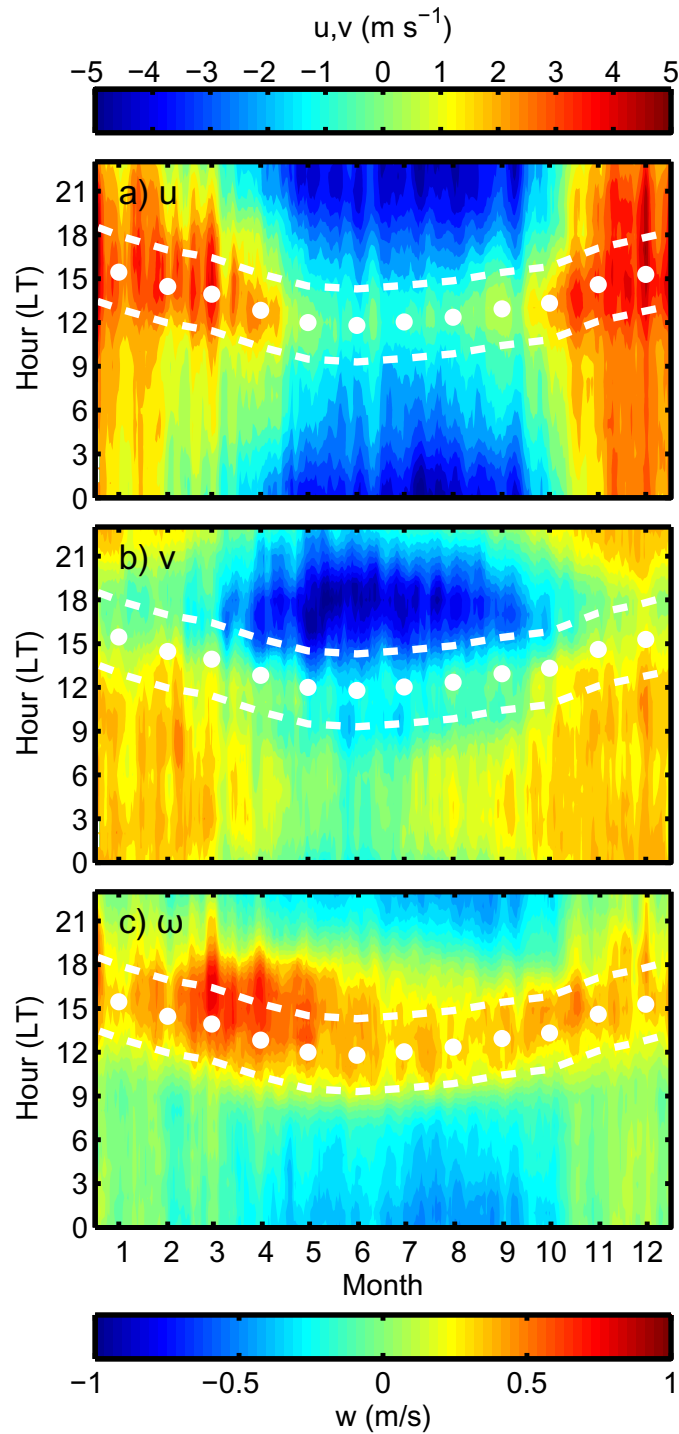


2

3 Figure 1 The location of the Mt. Waliguan GAW site and the two major cities in its vicinity.

4 The shading stands for the topographic height.

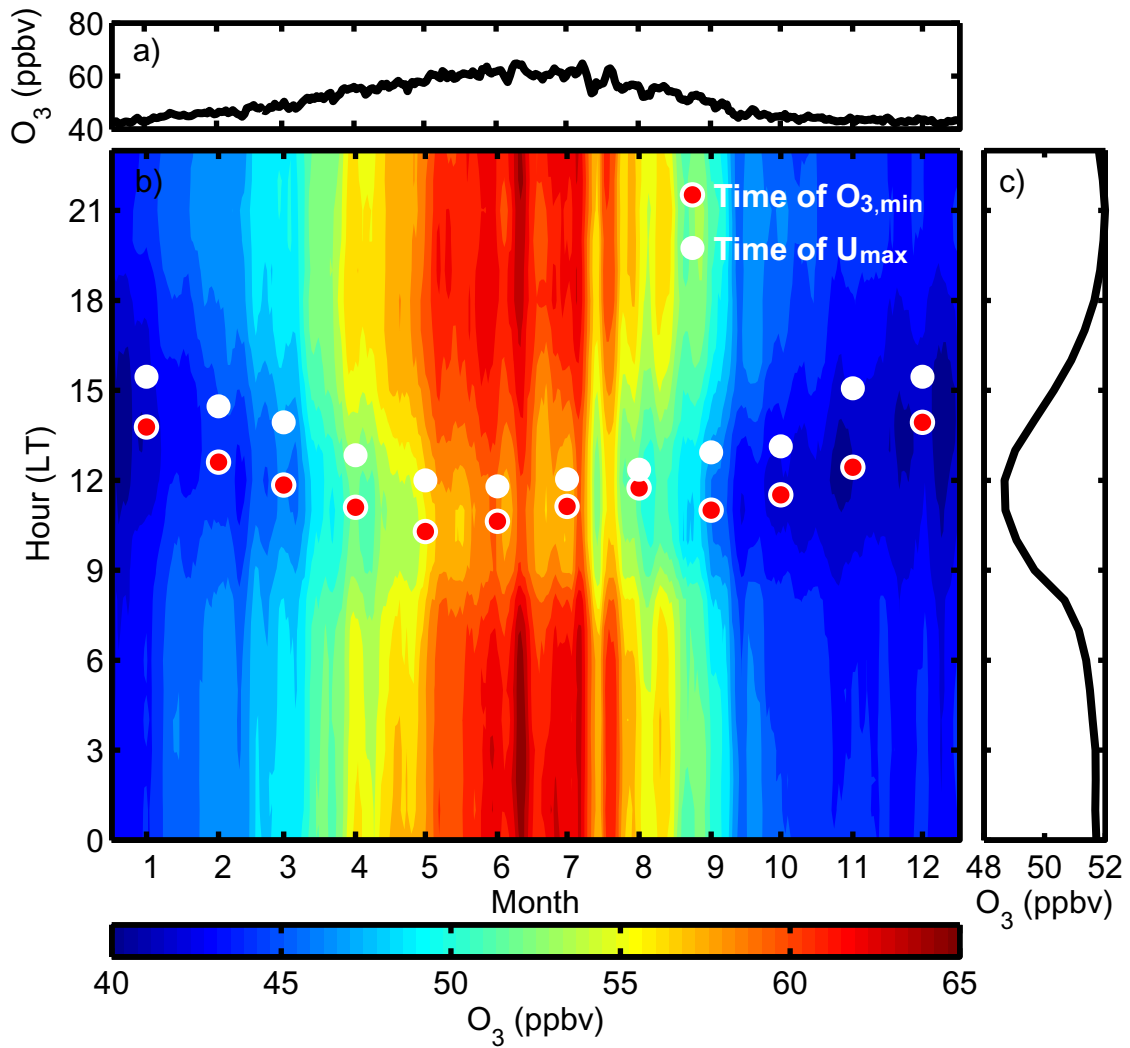
5



1

2 Figure 2 The average season-diurnal variation of surface zonal (a), meridional (b) and vertical
 3 (c) wind velocity on top of Mt. Waliguan during 1995-2013. The monthly average hour
 4 associated with the diurnal maximum zonal wind speed is given by the white dots, the daytime
 5 range is provided by the white dashed lines, which covers 6 hours centered around the white
 6 dots.

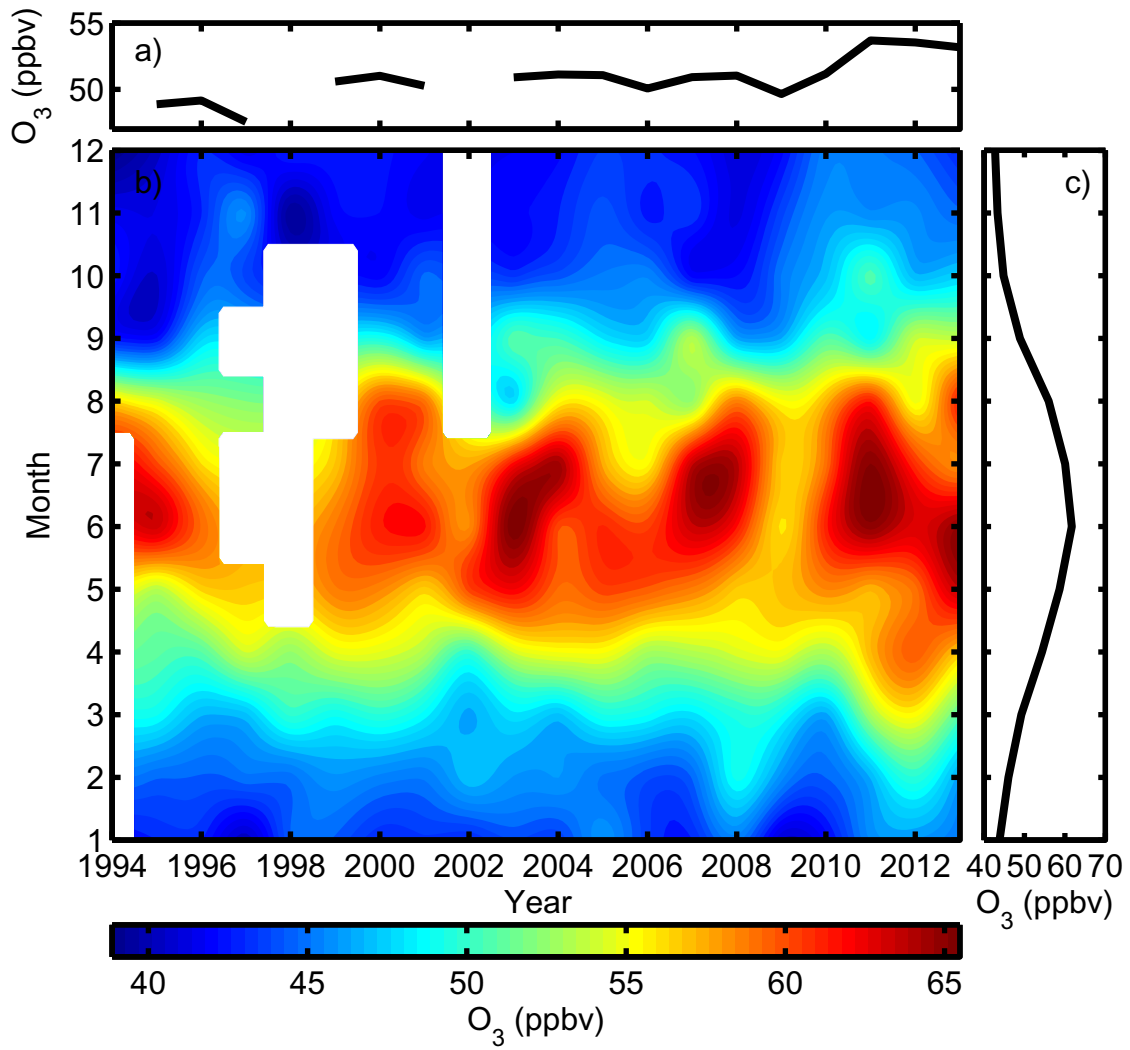
7



1

2 Figure 3 The average seasonal variation (a), season-diurnal variation (b) and diurnal variation
 3 (c) of ozone during 1995 to 2013. White dots stands for the monthly average local time
 4 associated with the diurnal minimum ozone, the white dashed line stands for a 6 hours range
 5 centered around the white dots.

6

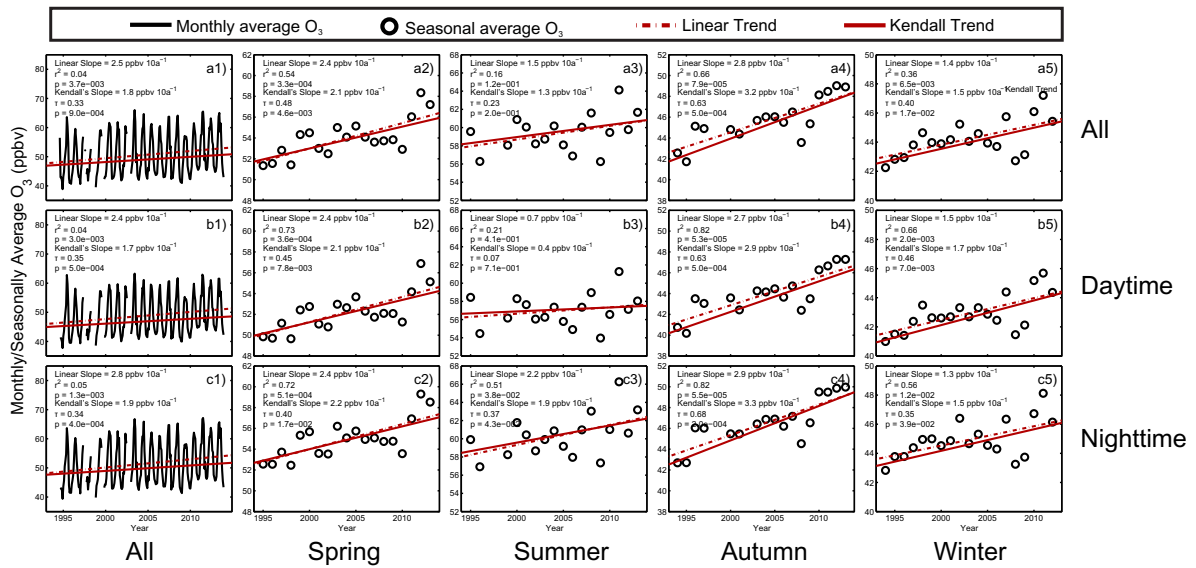


1

2 Figure 4 The average inter-annual variation (a), season-annual variation (b) and seasonal
 3 variation (c) of ozone during 1994 to 2013.

4

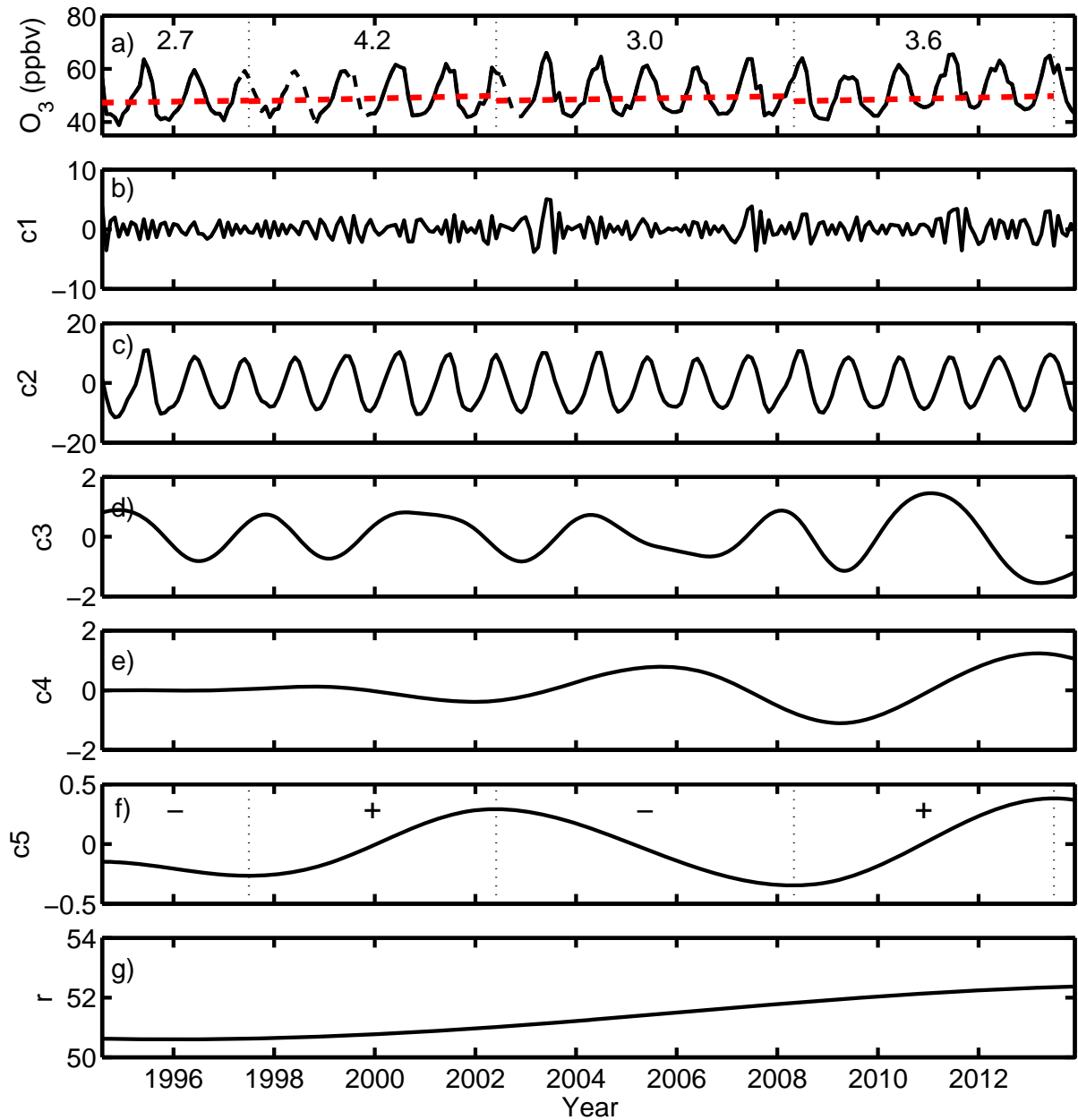
1



2

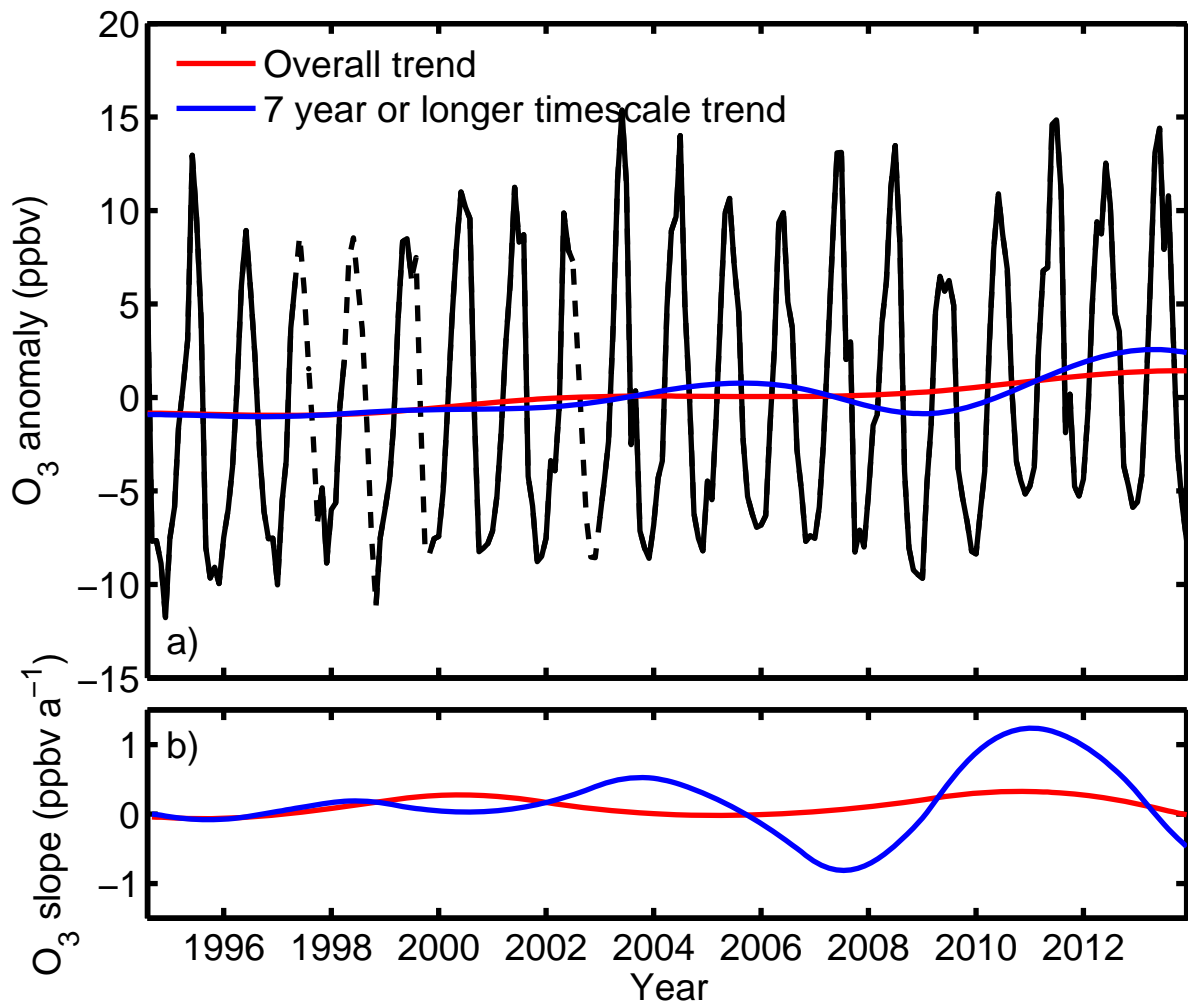
3 Figure 5 1) Monthly, 2) spring (MAM), 3) summer (JJA), 4) autumn (SON) and 5) winter time
 4 average all day (a), daytime (b) and nighttime (c) surface ozone mixing ratio during 1994 to
 5 2013 (black solid line or black circles) and its variation trend (red lines: dotted line stands for
 6 the linear variation and solid line stands for the Kendall's variation slope).

7



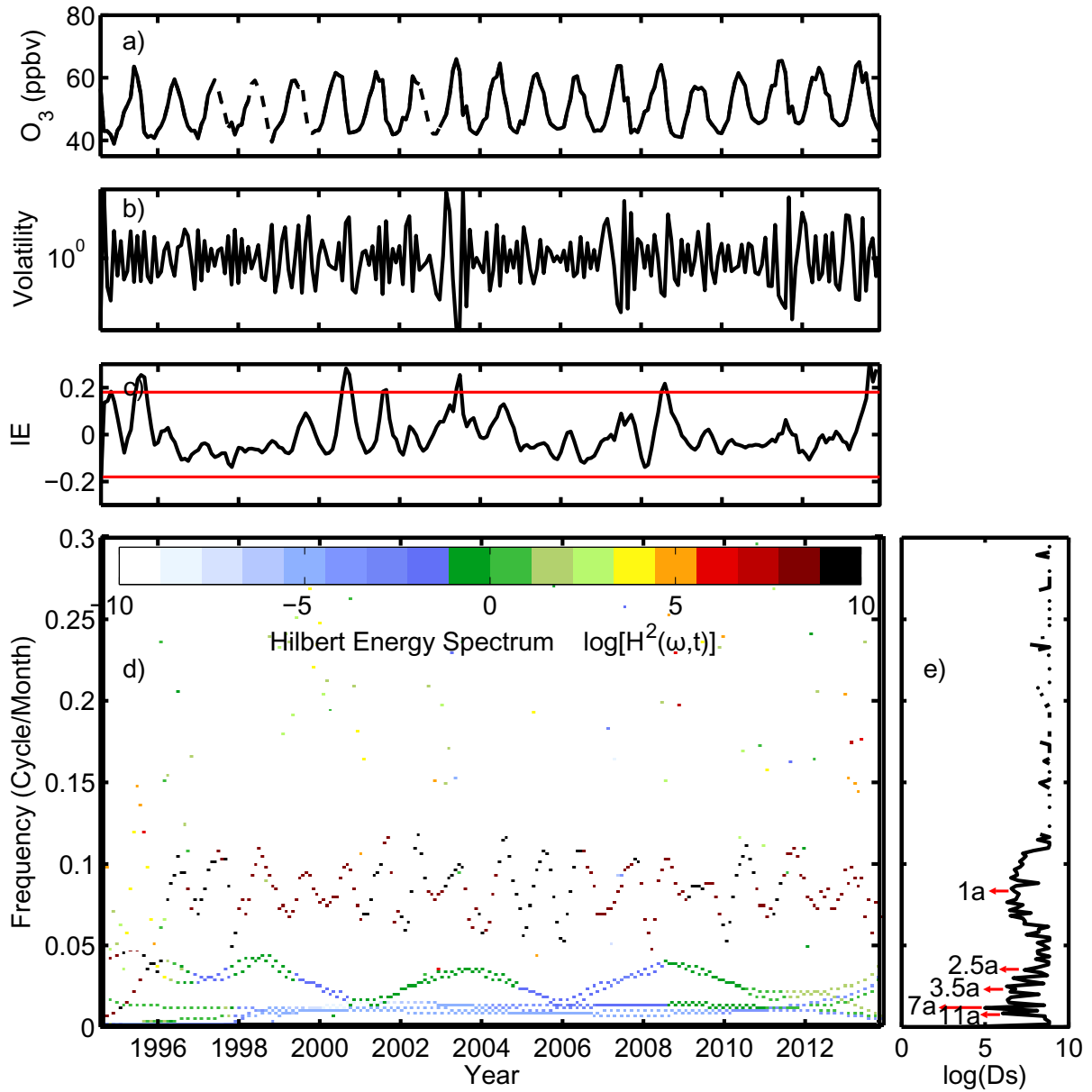
1
 2 Figure 6 The interpolated monthly average ozone mixing ratio at WLG from 1994 to 2013 (the
 3 interpolated data given in dashed lines, a) and its intrinsic mode functions c1-c5 (b-f, from the
 4 lowest order IMF to the highest order IMF) and its residue, r (g). The time segments in (a) were
 5 determined by the slope of the c5. The red slashed lines are the Kendall's trends and the
 6 numbers are the Kendall's slope (in ppbv $10a^{-1}$).

7



1
 2 Figure 7 a) The anomaly of the interpolated monthly average ozone (black line) the sum of last
 3 IMF and the residual (c5+r, red line) and the sum of the last two IMFs and the residual (c4+c5+r,
 4 blue line); b) the slope of the sum of last IMF and the residual (c5+r, red line) and the sum of
 5 the last two IMFs and the residual (c4+c5+r, blue line).
 6

1



2

3 Figure 8 The interpolated monthly average ozone mixing ratio signal at Mt. WLG during 1994
4 to 2013 (a), the volatility (b), the normalized mean value of the instantaneous energy (red lines:
5 $\pm 2\sigma$)(c), Hilbert Energy Spectrum (d) and the degree of stationarity (e).

6

7

8

9